Experimental and numerical studies on excess-air formation in quasi-saturated porous media

Stephan Klump,[1,2] Olaf A. Cirpka,[1] Heinz Surbeck,[3] and Rolf Kipfer[1,4]

Received 18 June 2007; revised 9 January 2008; accepted 5 February 2008; published 1 May 2008.

[1] The concentrations of conservative groundwater components of atmospheric origin often exceed the concentrations in equilibrium with the atmosphere. This phenomenon, called "excess air", is caused by gas exchange between entrapped gas and groundwater. We present experimental results from a horizontal quasi-saturated sand column, in which we have analyzed excess-air formation by noble-gas analysis and measurement of the total dissolved gas pressure. The experimental results agree with a numerical model based on kinetic dissolution of spherical gas bubbles. Parameter studies show that the dissolution of entrapped gas is controlled by gas-transfer kinetics only when the contact time between the water and gas phases is relatively short. In natural systems, this could be the case for gas exchange within the hyporheic zone of natural rivers. In the typical situation of excess-air formation upon regional groundwater recharge, it seems acceptable to apply gas-transfer models assuming local equilibrium. Additional parameter studies show that the direction of flow considerably affects the evolution of dissolution fronts. Our experimental and numerical results show that apparently unfractionated excess air is formed in the presence of a progressively dissolving gas phase, that is, the excess-air component has an elemental composition similar to that of free atmospheric air. This observation contradicts the common conceptual model that unfractionated excess air indicates the complete dissolution of entrapped air, as formulated in the unfractionated excess air (UA) model (Heaton and Vogel, 1981) which is also contained as a special case in the closed-system equilibrium (CE) model of Aeschbach-Hertig et al. (2000). We conjecture that the estimated fractionation factor, F, and amount of initial gas, A, determined by fitting the CE model to noble-gas concentrations, are biased when F is zero (apparently unfractionated excess air) and A corresponds to initial gas saturations smaller than one per cent.

Citation: Klump, S., O. A. Cirpka, H. Surbeck, and R. Kipfer (2008), Experimental and numerical studies on excess-air formation in quasi-saturated porous media, *Water Resour. Res.*, *44*, W05402, doi:10.1029/2007WR006280.

1. Introduction

[2] Gas exchange between groundwater and entrapped air within an otherwise water-saturated zone is of major significance for the transfer of atmospheric gases, such as molecular oxygen and nitrogen, into groundwater. A quasi-saturated zone, which is almost water-saturated but still contains entrapped residual gas, usually forms as the result of a rising groundwater table or due to air entrainment during water infiltration. Owing to the hydrostatic pressure, the aqueous-phase concentration of volatile compounds in equilibrium with the gas phase exceeds the solubility calculated for the ambient atmospheric pressure. In groundwater hydrology, the resulting supersaturation of dissolved atmospheric compounds is usually referred to as "excess air" [*Heaton and Vogel*, 1981].

[3] The occurrence of excess air is important in the interpretation of dissolved atmospheric compounds as environmental tracers. From concentrations of sulfur hexafluoride [*Busenberg and Plummer*, 2000] and chlorofluorocarbons [*Oster et al.*, 1996], groundwater samples can be dated because the atmospheric concentration has changed continuously over the past decades. Unrecognized excess air, causing higher concentrations than in equilibrium with the atmosphere, would lead to too young groundwater ages. In the determination of water age by the tritium-helium method, the atmospheric and terrigenic contributions must be subtracted from the measured ^{3}He concentrations [e.g., *Schlosser et al.*, 1988]. Again, ignoring excess air would lead to erroneous ratios of tritium to tritiogenic ^{3}He and thus erroneous ages. Most recently, excess air itself has been discussed as environmental tracer since variations in the amount of excess air reflect variations in physical conditions at the time of groundwater recharge [*Stute and Talma*, 1998; *Aeschbach-Hertig et al.*, 2002; *Beyerle et al.*, 2003; *Kulongoski et al.*, 2004; *Ingram et al.*, 2007; *Manning and Caine*, 2007]. Unfortu-

[1] Swiss Federal Institute of Aquatic Science and Technology (Eawag), Dübendorf, Switzerland.
[2] Now at EBA Engineering Consultants Ltd., Calcite Business Centre, Whitehorse, Yukon, Canada.
[3] Centre of Hydrogeology, University of Neuchâtel, Switzerland.
[4] Institute of Isotope Geochemistry and Mineral Resources, Zürich, Switzerland.

0043-1397/08/2007WR006280

nately, our current understanding of excess-air formation is insufficient to unambiguously relate excess-air values to climatic conditions at the time of recharge.

[4] Mass transfer between groundwater and entrapped gas is also important for the availability of dissolved oxygen in natural systems or in the operation of bio-sparging systems for groundwater remediation [e.g., *Johnson*, 1998]. Without recognition of excess air, the replenishment of oxygen in groundwater would notoriously be underestimated. Finally, gas exchange crucially affects the transport of volatile contaminants in groundwater [e.g., *Cirpka and Kitanidis*, 2001; *Amos and Mayer*, 2006].

[5] To quantify dissolution of entrapped gas in quasi-saturated media, it is advisable to study inert compounds of atmospheric origin. Perfect natural tracers for this purpose are noble gases [e.g., *Kipfer et al.*, 2002; *Holocher et al.*, 2002; *Klump et al.*, 2007]. The solubilities of noble gases in water depend on temperature and salinity. Because the dependence on temperature differs between the light and heavy noble gases, it is possible to determine the temperature of groundwater at the time of recharge from the composition of dissolved noble gases [e.g., *Mazor*, 1972]. Excess air has the strongest effect on He and Ne concentrations due to their low solubilities. Because He is additionally produced in radioactive processes, typically Ne, which in meteoric water is of pure atmospheric origin, is used to quantify excess air in groundwater. The geochemical literature contains conceptually simple models of excess air formation assuming equilibrium between water and gas bubbles in a closed system. The bubbles may be dissolved completely or only partially. These models are widely used to interpret measured noble gas concentrations in terms of the temperature during recharge, the initial amount of entrapped air, and the degree of gas dissolution [*Heaton and Vogel*, 1981; *Stute et al.*, 1995; *Aeschbach-Hertig et al.*, 2000]. From a principal point of view, these models are conceptually incorrect when applied to systems with moving water, in which dissolution fronts can evolve with chromatography-like separation of more and less soluble volatile compounds [*Cirpka and Kitanidis*, 2001]. A particular objective of the current study is to analyze what type of errors are induced by interpreting dissolved noble gas concentrations in a system with advective transport by models derived for a closed system. Such an analysis is necessary because typically the history of a water sample within the aquifer is not known in practical applications. In paleoclimatic studies, for instance, typically a few groundwater samples of potentially high age are taken and analyzed in order to reconstruct the climatic conditions at the time of recharge. If some parameters derived by the interpretive geochemical models [*Aeschbach-Hertig et al.*, 2000], such as the soil temperature at the time of recharge, are reliable despite the incorrect underlying assumptions, these robust parameters may be used for further analysis. Derived parameters that are very sensitive to assumptions about transport, however, should be handled with extreme care.

[6] *Holocher et al.* [2002, 2003] and *Geistlinger et al.* [2005] investigated gas exchange and the formation of excess air in quasi-saturated porous media using sand-column experiments in conjunction with numerical simulations of solute transport coupled to dissolution of an immobile gas phase. On the basis of these results, we conducted further systematic sand-column experiments. Our work addresses several questions which were posed in the previous studies but have not yet been answered sufficiently well. These questions concern: (i) the role of kinetic effects on the dissolution of entrapped air; (ii) the effect of the spatial orientation of flow; and (iii) the formation of apparently unfractionated excess air, i.e., a gas surplus which has the same elemental composition as free atmospheric air, despite clear evidence of incomplete and ongoing gas dissolution. In more detail, these questions involve the following aspects:

[7] (i) There are different gas-exchange models available, which simulate the physical processes governing air/water partitioning in porous media between a mobile water phase and an immobile, trapped gas phase. These models either consider the kinetics of the dissolution of entrapped gas (e.g., kinetic bubble dissolution (KBD) model [*Holocher et al.*, 2003]) or assume local equilibrium between water and gas (e.g., local equilibrium model) [*Cirpka and Kitanidis*, 2001]. Because the computational effort of the local equilibrium model is much smaller than that of the KBD model, we want to determine under which conditions the assumption of local equilibrium is acceptable.

[8] (ii) *Holocher et al.* [2002] performed laboratory experiments in vertical sand columns with downward flow, whereas *Geistlinger et al.* [2005] conducted similar column experiments applying upward flow. Because hydrostatic pressure controls the gas equilibrium in quasi-saturated porous media, horizontal flow (with quasi-constant hydrostatic pressure in the direction of flow) is conceptually different from vertical flow (where pressure increases or decreases with travel distance). As the natural flow direction of groundwater is mostly horizontal, the differences between vertical and horizontal water flow are of great importance for understanding gas exchange in natural porous media.

[9] (iii) In sand-column experiments, *Holocher* [2002] observed the formation of apparently unfractionated excess air, i.e., the elemental composition of the excess air component was very similar to atmospheric air, even in the presence of a partially dissolved gas phase. *Holocher et al.* [2002] did not analyze this observation in further detail, although it contradicts the original conceptual assumption that unfractionated excess air is the result of completely dissolving the entrapped air.

2. Theory

2.1. Gas-Water Equilibrium

[10] Atmospheric compounds are incorporated into groundwater by gas exchange between the water and the atmosphere or soil air. The dissolution of atmospheric compounds in natural water can reasonably be described by Henry's Law:

$$c_i^{eq} = \frac{p_i}{R \cdot T \cdot K_{H,i}(T,S)} \tag{1}$$

in which c_i^{eq} is the equilibrium concentration of compound i, p_i is the partial pressure of that compound in the

atmosphere, R is the universal gas constant, $K_{H,i}$ is the dimensionless Henry's law coefficient of compound i, T is absolute temperature, and S denotes salinity.

[11] The solubilities of the noble gases increase with atomic mass from He to Xe [*Weiss*, 1970, 1971; *Weiss and Kyser*, 1978; *Clever*, 1979]. The strongly temperature-dependent solubilities of the heavy noble gases Ar, Kr, and Xe allow reconstructing the temperature that prevailed during infiltration [e.g., *Mazor*, 1972]. The light and least soluble noble gases He and Ne react most sensitively to the presence of excess air, and are therefore used to quantify the excess air component in groundwater samples. In addition to atmospheric He, groundwater often contains non-atmospheric He, which is produced by the radioactive decay of U and Th or accumulates due to He emanation from different geochemical reservoirs within the earth. Excess air is often expressed in terms of relative Ne supersaturation (ΔNe); i.e., the Ne excess as a percentage of its atmospheric equilibrium concentration (c^{eq}_{Ne}):

$$\Delta\mathrm{Ne} = \frac{c_{\mathrm{Ne}} - c^{eq}_{\mathrm{Ne}}}{c^{eq}_{\mathrm{Ne}}} \tag{2}$$

2.2. Geochemical Models of Excess-Air Formation

[12] Simplified conceptual models have been developed to interpret measured concentrations of dissolved gas components. In the simplest of these models (unfractionated excess air (UA) model), excess air originates from complete dissolution of a gas body, which originally had atmospheric composition [*Heaton and Vogel*, 1981]. This model has been modified to account for diffusive mass transfer between the water body containing excess air and the atmosphere [*Stute et al.*, 1995], partial dissolution of the gas phase [*Aeschbach-Hertig et al.*, 2000], both leading to fractionated excess air, and for capillary pressure of the remaining gas phase [*Mercury et al.*, 2004].

[13] According to the closed-system equilibration (CE) model, the formation of excess air results from the equilibration of a finite water volume with a finite air volume at increased hydrostatic pressure within the quasi-saturated zone [*Aeschbach-Hertig et al.*, 2000]:

$$c_i(T,S,p_{atm},A,F) = c_i^{eq}(T,S,p) + \frac{(1-F)\cdot A\cdot z_i\cdot c_i^{eq}(T,S,p)}{c_i^{eq}(T,S,p) + F\cdot A\cdot z_i} \tag{3}$$

The initial amount of entrapped air is given by A, whereas the fractionation parameter F describes the reduction of this initial gas volume due to dissolution and compression. The parameter z_i is the volume fraction of component i in dry air.

[14] Unfractionated excess air, characterized by $F = 0$, reflects complete dissolution of the entrapped air. If the hydrostatic pressure is not sufficient for complete dissolution, the compositions of both the dissolved gas and the remaining gas phase are fractionated; i.e., the elemental composition differs from that of pure atmospheric air [e.g., *Kipfer et al.*, 2002]. Because of their high solubilities, the heavy noble gases Ar, Kr and Xe are enriched in the water phase relative to the poorly soluble, light noble gases He and Ne.

[15] The fractionation factor F, ranging from zero (complete dissolution of the gas phase) to one (no dissolution at all) is defined by:

$$F = \frac{v_{CE}}{q_{CE}} \text{ with } v_{CE} = \frac{V_g}{V_g^{ini}} \text{ and } q_{CE} = \frac{p_g - p_w}{p_{atm} - p_w} \tag{4}$$

in which V_g and V_g^{ini} are the volumes of the remaining gas phase and the initial gas phase prior to compression, respectively, p_w is the water-vapor pressure, and p_g is the total gas pressure in the remaining gas phase. The pressure factor q_{CE} is the ratio of the dry gas pressure in the entrapped gas phase to that in the free atmosphere and thus, q_{CE} is a measure of the hydrostatic pressure exerted on the entrapped air.

[16] Typically, more air is entrapped in the soil matrix than can be dissolved in the surrounding water phase at the prevailing pressure, which is the sum of atmospheric, hydrostatic and capillary pressures. If solubility equilibrium between the water and entrapped air is achieved, the fractionation of the resulting excess air component is therefore similar to that described by the CE model, and its size, expressed in natural systems as ΔNe (equation (2)), is limited by the pressure acting on the entrapped air.

[17] Usually, some of the free model parameters of the CE model are well constrained in groundwater studies. For example, S is commonly negligibly low in fresh groundwater and p_{atm} is defined by the altitude of the recharge area. The remaining parameters T, A, and F can be determined from the measured Ne, Ar, Kr, and Xe concentrations by numerical inversion of equation (3) [*Aeschbach-Hertig et al.*, 1999; *Ballentine and Hall*, 1999].

2.3. Numerical Models of Gas Exchange Coupled to Advective-Dispersive Transport

[18] The models mentioned in section 2.2 do not consider advective-dispersive transport of volatile compounds in the aqueous phase. In the following, we review two models in which partitioning between groundwater and entrapped gas is coupled to solute transport in water. We present both models in a one-dimensional setup, but they can easily be extended to two or three dimensions. As volatile compounds, we consider the noble gases He, Ne, Ar, Kr, and Xe, and the two main air constituents N_2 and O_2. Chemical and radioactive transformations are neglected. In natural systems, the non-conservative behavior of certain gases, e.g., the consumption of O_2 by aerobic respiration, or the production of N_2, CO_2, and CH_4 by denitrification, oxidation of organic carbon, and methanogenesis, respectively, may have to be considered. For example, *Balcke et al.* [2007] investigated kinetic gas-water transfer during air sparging in sand-column experiments, and *Amos and Mayer* [2006] analyzed gas partitioning in methanogenic systems. *Williams and Oostrom* [2000] examined oxidation of anoxic water by oxygen transfer upon water table fluctuations. The mentioned processes are particularly important when they change major contributions to the sum of partial pressures. Such considerations, however, are beyond the scope of the present study.

2.3.1. Local Equilibrium Model

[19] In the local equilibrium model, we assume that the immobile gas phase and the mobile water phase are locally

in physicochemical equilibrium [*Cirpka and Kitanidis*, 2001]. Kinetic effects of inter-phase mass transfer are neglected so that gas exchange is controlled solely by the different gas solubilities and not by the molecular diffusivities of the volatile compounds. Mass conservation of a single compound i requires:

$$\Theta \frac{\partial c_{i,tot}}{\partial t} + \frac{\partial}{\partial x}\left(q c_i - \Theta D \frac{\partial c_i}{\partial x}\right) = 0 \tag{5}$$

with porosity Θ, the specific-discharge q, the aqueous-phase concentration c_i, and the dispersion coefficient D. $c_{i,tot}$ denotes the total concentration of compound i, that is, the mass summed over all phases per pore volume, which can be computed as:

$$c_{i,tot} = S_g \cdot c_i^g + (1 - S_g) \cdot c_i \tag{6}$$

which c_i^g is the volumetric concentration of compound i in the gas phase, and S_g is the gas saturation, i.e., the fraction of the pore volume occupied by gas.

[20] Neglecting the compressibility of water and pore space, the continuity equation can be expressed as:

$$\frac{\partial q}{\partial x} = \Theta \frac{\partial S_g}{\partial t} \tag{7}$$

[21] Equations (5)–(7) hold for both kinetic and instantaneous gas transfer. In the local equilibrium model, we assume that Henry's law holds throughout the domain at all times:

$$c_i^g = K_{H,i} \cdot c_i \tag{8}$$

Considering the ideal gas law for all gas components to relate volumetric gas concentrations c_i^g to partial pressure and summing up all partial pressures leads to the total gas pressure p_g:

$$p_g = p_w + R \cdot T \cdot \sum_i c_i^g \tag{9}$$

which is also defined as the the sum of the pressure p_{aq} in the aqueous phase and the capillary pressure p_c:

$$p_g = p_{aq} + p_c \tag{10}$$

Assuming that the gas phase is made of spherical bubbles with radius r, the gas pressure p_g can be computed by:

$$p_g = p_{atm} + \rho \cdot g \cdot (h - z) + 2\sigma \cdot \left(\frac{V_{por}}{n_b} \cdot \frac{3 S_g}{4\pi}\right)^{-1/3} \tag{11}$$

in which ρ is the mass density of water, $g = 9.81$ m/s^2 is the acceleration constant due to gravity, h is hydraulic head, z is the geodetic height, and σ is the surface tension of water. n_b/V_{por} denotes the number of gas bubbles per pore volume.

[22] We solve the coupled system of equations by an operator-split method. Within a time step, we first solve for advective-dispersive transport in the aqueous domain by a Finite-Volume discretization in space and implicit Euler integration in time, keeping the gas phase constant. Subsequently, we re-equilibrate the aqueous and gaseous phases. Combining equations (6), (8), and (9), we can compute the gas pressure p_g as function of the gas saturation S_g for given total concentrations $c_{i;tot}$. This gas pressure must equal the value given by equation (11). We determine the corresponding value of S_g by Newton-Raphson iteration.

2.3.2. Kinetic Bubble Dissolution (KBD) Model

[23] In the kinetic bubble dissolution (KBD) model of *Holocher et al.* [2003], the kinetic mass transfer between the air phase, assumed to consist of spherical bubbles, and the water phase is modeled by a water-side boundary layer gas-exchange approach. Here, the mass-flux J_i of compound i per surface area of a bubble is assumed proportional to the saturation surplus of the aqueous-phase concentration with respect to the gas-phase concentration:

$$J_i = k_i \cdot \left(c_i - \frac{c_i^g}{K_{H,i}}\right) \tag{12}$$

in which a positive flux is from the aqueous to the gaseous phase, and k_i is the mass transfer coefficient of compound i approximated by [*Epstein and Plesset*, 1950]:

$$k_i = D_{w,i} \cdot \left(\frac{1}{r} + \sqrt{\frac{v}{2\pi r \cdot D_{w,i}}}\right) \tag{13}$$

with the molecular diffusion coefficient $D_{w,i}$ of compound i in water and the seepage velocity $v = q/(1 - S_g)/\Theta$. The total flux from the aqueous phase to a single bubble is given by multiplying J_i with the surface area of the bubble. Summation over all compounds and consideration of the ideal gas law leads to the rates of change of the bubble radius r and the gas saturation S_g:

$$\frac{dr}{dt} = \frac{R \cdot T}{p_g - \frac{2\sigma}{3r}} \sum_i J_i \tag{14}$$

$$\frac{dS_g}{dt} = 4\pi \cdot r^2 \cdot \frac{n_b}{V_{por}} \cdot \frac{dr}{dt} \tag{15}$$

in which p_g is given by equation (11).

[24] In contrast to the local equilibrium model, the conservation equation for the total concentration, equation (5), must be split into equations for the concentrations in the aqueous and gaseous phases, respectively:

$$\Theta \frac{\partial((1 - S_g) \cdot c_i)}{\partial t} + \frac{\partial}{\partial x}\left(q c_i - \Theta D \frac{\partial c_i}{\partial x}\right) = -\Theta \frac{d(S_g \cdot c_i^g)}{dt} \tag{16}$$

$$\frac{d(S_g \cdot c_i^g)}{dt} = 4\pi \cdot r^2 \cdot \frac{n_b}{V_{por}} \cdot J_i \tag{17}$$

in which the transport equations of all individual volatile compounds are coupled by the pressure constraint of equation (9).

[25] In the numerical implementation, the aqueous-phase concentrations c_i and the number of moles in the gaseous phase per pore volume, $c_i^g \cdot S_g$, are used as primary

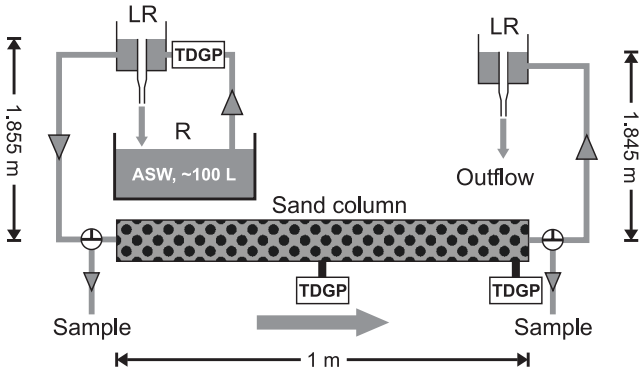

Figure 1. Experimental set-up for the sand-column (length: 1 m, diameter: 5.2 cm) experiment. About 100 L of air-saturated water (ASW) was prepared in an open reservoir (R). The hydraulic heads at both ends of the column were kept constant making use of leveling reservoirs (LR). Water samples for the analysis of dissolved noble gases could be taken at both inflow and outflow of the column. Total dissolved gas pressure (TDGP) was measured in the inflowing water, in the middle, and at the end of the column.

unknowns. The transport terms of equation (16) are discretized by the Finite Volume method, and the resulting system of ordinary differential equations is solved by Gear's method (MATLAB® function ode15s). For a more detailed description of the KBD model see *Holocher et al.* [2003].

3. Experimental Methods

3.1. Experimental Set-Up

[26] We performed a laboratory experiment using a packed sand column in order to test the validity of the local equilibrium and KBD models and to relate the interpretation of noble gas concentrations by the CE model to known hydraulic conditions. The experimental set-up is shown in Figure 1. The acrylic glass column had a length of 1 m and an inner diameter of 5.2 cm. It was equipped with sampling ports at both the inflow and outflow of the column. The column was packed with clean, well-sorted quartz sand with a grain size of 1.6 to 2.5 mm (Dorsilit® Nr.5G, Dorfner). The column was installed horizontally. As boundary conditions, we applied constant heads of 1.855 m and 1.845 m to the in- and outflow, respectively, which resulted in a hydraulic gradient of 0.01.

[27] The sand column was filled vertically from the bottom to the top with air-equilibrated water. During the filling process, residual air was entrapped in the column. After the column had been filled completely, it was turned into a horizontal position and connected to one of the leveling reservoirs leading to a hydraulic head of about 1.85 m. To allow re-equilibration of the water and the entrapped gas phase, flow was started not until 3 h after filling the column.

[28] We used local tap-water which had been equilibrated with the atmosphere by slowly stirring it in an open reservoir (V $\approx$ 100 L) for about one week. To ensure complete equilibration, the water was analyzed for dissolved noble gases prior to the experiment. Biological consumption of oxygen was prevented by adding about 10 mg/L chlorine dioxide. The experiment was conducted in a climatized room with a constant air temperature of 20°C and a constant relative humidity of 90%. The mean atmospheric pressure was 9.691×10^4 Pa.

[29] At time zero (3 h after connecting the column to one of the leveling reservoirs), flow was initiated by connecting also the other reservoir. The inflowing water was in gas equilibrium with the atmosphere, whereas the pressure of both water and entrapped gas in the column was about 18'500 Pa higher than the atmospheric pressure. Thus the column was continuously flushed with water that was undersaturated with respect to the gas/water equilibrium within the column, leading to dissolution of the entrapped air.

[30] Water samples for the analysis of dissolved noble gases were taken both from the inflow and outflow of the column during the experiment, which lasted about 46 h. Water samples (22.5 mL) were put into copper tubes, which were then sealed gas-tight by pinch-off clamps, following the standard sampling procedure [*Beyerle et al.*, 2000]. The abundances of the dissolved noble gases He, Ne, Ar, Kr, and Xe were analyzed by mass spectrometry in the Noble Gas Laboratory at ETH Zurich [*Beyerle et al.*, 2000]. The accuracy of the noble-gas analysis is listed in the caption of Table 1.

3.2. Hydraulic Parameter Identification

[31] We determined the seepage velocity $v = q/\Theta$ and the dispersion coefficient D by a conservative-tracer experiment using sodium chloride. The tracer was injected continuously into the inflow of the column, while the breakthrough curve was recorded at the outflow by quasi continuously measuring the electrical conductivity (temporal resolution: 1 min). The applied tracer dosage increased the electrical conductivity only slightly from about 800 mS/cm to about 1150 mS/cm. In the range of applied salt-tracer concentrations, buoyancy effects of the tracer test can be excluded. The parameters v and D were determined by fitting the analytical solution for stepwise injection to the data [*Kreft and Zuber*, 1978]:

$$c_n(L,t) = \frac{EC(L,t) - EC_0}{EC_{in} - EC_0} = \frac{1}{2} \cdot \mathrm{erfc}\left(\frac{L - v \cdot t}{\sqrt{4D \cdot t}}\right) + \frac{1}{2} \cdot \exp\left(\frac{v \cdot L}{D}\right) \cdot \mathrm{erfc}\left(\frac{L + v \cdot t}{\sqrt{4D \cdot t}}\right) \quad (18)$$

in which c_n is normalized concentration, $EC(L,t)$ is the measured electric conductivity at the outlet, EC_{in} that in the injected solution, and EC_0 that before application of the tracer. L is the length of the column. Fitting was done by minimizing the squared residuals using the Nelder-Mead simplex algorithm implemented in MATLAB® [*Lagarias et al.*, 1998].

[32] The porosity Θ can be determined according to:

$$\Theta = \frac{q}{v} = \frac{Q}{v \cdot A_{col}} \quad (19)$$

where q is the Darcy velocity (specific discharge), Q is the total volumetric flow, and A_{col} is the cross-sectional area of the column.

Table 1. Noble Gas Concentrations and Isotope Ratios in the Water Samples From the Sand Column Experiment[a]

No.	Time [h]	He [10^{-8}]	Ne [10^{-7}]	Ar [10^{-4}]	Kr [10^{-8}]	Xe [10^{-9}]	^{3}He/^{4}He [10^{-6}]	^{22}Ne/^{20}Ne [−]	^{40}Ar/^{36}Ar [−]
					Inflow				
I1	0.00	4.36	1.78	3.01	6.62	9.14	1.38	0.1023	295.3
I2	20.00	4.34	1.77	2.99	6.57	9.19	1.36	0.1021	296.1
I3	46.00	4.35	1.77	2.98	6.55	9.05	1.38	0.1020	296.2
					Outflow				
1	0.00	5.13	2.09	3.42	7.38	9.97	1.37	0.1022	295.7
2	5.25	5.53	2.23	3.26	6.93	9.45	1.37	0.1020	295.9
3	11.50	5.82	2.25	3.20	6.86	9.40	1.38	0.1019	295.5
4	15.00	5.63	2.19	3.17	6.78	9.36	1.37	0.1021	295.5
5	17.50	5.39	2.11	3.13	6.69	9.00	1.37	0.1023	295.8
6	22.50	4.95	1.98	3.08	6.68	9.29	1.36	0.1019	296.0
7	27.50	4.51	1.83	3.01	6.59	9.26	1.37	0.1020	295.1
8	34.00	4.36	1.78	3.00	6.56	9.22	1.37	0.1019	295.2
9	42.25	4.33	1.75	2.99	6.60	9.15	1.36	0.1021	295.1

[a]The samples I1 – I3 were taken from the inflow of the column, the samples 1 – 9 from the outflow of the column. All noble gas concentrations are given in cm^3_{STP}/g. The overall measurement errors (1σ errors) are ±1% for He, Ne, and Ar, ±1.5% for Kr, ±2% for Xe, ±0.7% for ^{3}He/^{4}He, ±0.3% for ^{22}Ne/^{20}Ne, and ±0.2% for ^{40}Ar/^{36}Ar.

[33] The hydraulic conductivity K can be estimated as follows:

$$K = \frac{q}{I} \tag{20}$$

with $I = 0.01$ being the hydraulic gradient (see Figure 1).

[34] The resulting parameter values were $D = 2.58 \times 10^{-6}$ m^2/s for the dispersion coefficient, $v = 2.95 \times 10^{-4}$ m/s for the mean seepage velocity, $K = 1.18 \times 10^{-2}$ m/s for the hydraulic conductivity, and $\Theta = 0.4$ for the porosity.

3.3. Total Dissolved Gas Pressure (TDGP) Probes

[35] In addition to the analysis of dissolved noble gases, total dissolved gas pressure (TDGP) probes were used to measure the total content of dissolved gases in the column during the experiment. The TDGP probe consists of a gas-permeable silicone-rubber tube (length: 10 cm, outer diameter: 2 mm, inner diameter: 1 mm) with a pressure transducer attached at one end. The other end of the tube is knotted tightly to close it off. Two tubes are rolled up in a spiral and installed directly into the sand at the outflow of the column. The pressure transducer is connected to the silicone-rubber tubes via short stainless-steel cannulas (length: 1 cm) which are led through the acrylic glass wall of the column. In addition, a further TDGP probe was installed in the inflow of the column to measure the TDGP in the inflowing water.

[36] The gas volume inside the silicone-rubber tube's void is in gas exchange with the surrounding water phase, and the total gas pressure inside the tube is measured relative to the ambient atmospheric pressure. The equilibration time of the TDGP probe is approximately 15 min [unpublished data of H. Surbeck; *Manning et al.*, 2003]. If the sum of the partial pressures of the dissolved gases in the water exceeds the atmospheric solubility equilibrium pressure, the total pressure inside the tube must exceed the atmospheric pressure. As the partial pressures of N_2 and O_2 amount to about 99% of the total pressure in atmospheric air, the TDGP signal in water is usually given essentially by the sum of the partial pressures of these two gases.

[37] The main advantage of the TDGP probe is its ability to measure the total dissolved gas content of the water in a quasi-continuous mode. During the experiment, the TDGP of the water was measured every 30 min.

4. Experimental Results

4.1. Dissolved Noble Gas Concentrations

[38] The concentrations of noble gases in the samples taken during the sand-column experiment are listed in Table 1. Like in field studies, the data were interpreted by the closed-system equilibration (CE) model of *Aeschbach-Hertig et al.* [2000], resulting in apparent values of the noble gas temperature T_{ng}, the amount A of entrapped air, and the fractionation factor F of the excess air component (see section 2.2 and Table 2).

[39] Samples I1 – I3 were taken in the reservoir of water used for injection into the column. This water was close to equilibrium with the atmosphere ($\|c_i - c_i^{eq}\|/c_i^{eq} < 0.02$), the concentrations were approximately constant, and the deter-

Table 2. Noble Gas Temperature T_{ng}, Apparent Amount of Entrapped Air A, and Fractionation Factor F of the Water Samples From the Sand-Column Experiment as Determined by UA or CE Models, Respectively[a]

No.	Time, h	T_{ng}, °C	A, cm_{STP}^3/kg	F [−]
		Inflow		
I1	0.00	20.2 ± 0.1	0.16 ± 0.03	0
I2	20.00	19.8 ± 0.1	0.15 ± 0.03	0
I3	46.00	20.0 ± 0.1	0.13 ± 0.03	0
		Outflow		
1	0.00	22.0 ± 0.9	311 ± 268	0.82 ± 0.00
2	5.25	20.1 ± 0.4	7.55 ± 2.32	0.52 ± 0.08
3	11.50	20.5 ± 0.2	2.90 ± 0.04	0
4	15.00	20.5 ± 0.2	2.54 ± 0.04	0
5	17.50	20.9 ± 0.2	2.12 ± 0.04	0
6	22.50	20.2 ± 0.2	1.29 ± 0.04	0
7	27.50	20.1 ± 0.1	0.44 ± 0.03	0
8	34.00	20.0 ± 0.1	0.18 ± 0.03	0
9	42.25	19.9 ± 0.1	0.07 ± 0.03	0

[a]Only for the samples no. 1 and 2, the UA model did not yield any acceptable fit. Therefore these two samples were fitted using the CE model. Note that the UA model is also included in the CE model as a special case for $F = 0$.

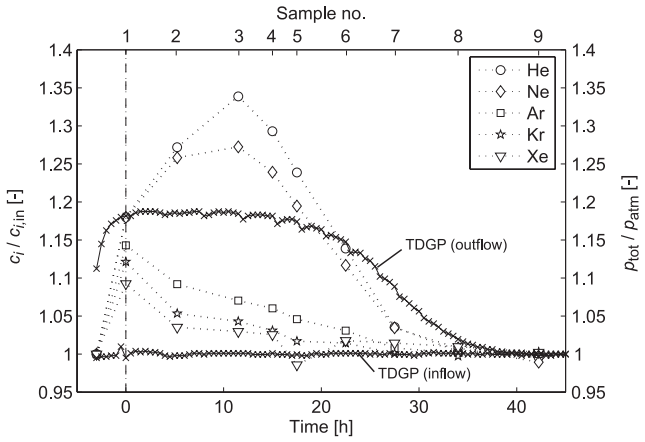

Figure 2. Measured dissolved noble gas concentrations and total dissolved gas pressures (TDGP) during the sand-column experiment. All noble gas concentrations are normalized by their respective concentrations in the inflowing water. The TDGPs are normalized by the ambient atmospheric pressure.

mined noble gas temperature T_{ng} = 20.0 ± 0.2°C was identical to the constant ambient air temperature of 20°C. The noble gas temperatures T_{ng} determined in samples taken during the experiment from the outflow of the column were less than 1 K higher than the real water temperature (cf. Table 2). We conclude that the noble gas temperature T_{ng} was a reliable indicator of the true water temperature in our experiment.

[40] Figure 2 shows the evolution of the noble gas concentrations during the column experiment. After filling the column at $t = -3$ h, the initially air-equilibrated water dissolved part of the entrapped air, leading to the observed supersaturation of 10–20% at $t = 0$ *h*. After initiation of the water flow at $t = 0$ *h*, the concentrations of the light noble gases He and Ne continued to increase, whereas the concentrations of the heavy noble gases Ar, Kr, and Xe decreased. This is so because Ar, Kr, and Xe have significantly higher solubilities than He and Ne. With respect to atmospheric air, the entrapped air therefore became enriched in He and Ne, and depleted in Ar, Kr, and Xe. Later, at about $t = 15$ *h*, all noble gas concentrations decreased due to the progressively dissolving gas phase. After about 35 *h*, the entrapped air was virtually completely dissolved by the water flowing through the column, which is indicated by concentrations in the outflow being approximately identical to those in the inflow.

[41] Figure 3 shows the evolution of the He and Ar concentrations during the experiment. The first two samples, taken at $t = 0$ *h* and $t = 5.25$ *h* (see Figures 2 and 3) contain excess air components which appear fractionated with respect to pure atmospheric air if applying the CE model for interpretation (values of $F > 0$, listed in Table 2). All other samples (3–9; see Figures 2 and 3) are interpreted to contain pure, unfractionated excess air, yielding the best fits for $F = 0$. The time needed to flush the column is about 1 h. That is, after the column had been flushed about 5–10 times, the transition occurred from fractionated to apparently unfractionated excess air, and after the column had been flushed about 30 times, the entrapped air was dissolved completely.

[42] The shift of samples 3–6 toward a slightly higher temperature can be explained by a small relative excess of the least soluble gases (He, Ne) with respect to the better soluble noble gases Ar, Kr, and Xe (cf. section 5.3). As described below, this relative surplus of the least soluble (noble) gases is characteristic for apparently unfractionated excess air formed during the later stage of bubble dissolution.

[43] The observation that the excess air component is fractionated during the early stage of gas dissolution and apparently unfractionated at later times during the experiment is in agreement with results of *Holocher et al.* [2002]. The samples containing apparently unfractionated excess air were taken in the presence of a dissolving gas phase, contradicting the classical interpretation of unfractionated excess air, which is assumed to result from complete dissolution of entrapped air. The associated amount A of excess air determined by the UA model (or by the special UA-case of the CE model for $F = 0$) corresponds to an initial gas saturation of <0.3%. The numerical simulations of reactive transport discussed below show that these values are much too small. That is, the fractionation factor F and the amount of excess air A determined by the CE model are sensitive to the conceptual assumption of a closed system and must be handled with care. In section 5.3, we will assess the occurrence of apparently unfractionated excess air in more detail.

[44] To gain a better understanding of the underlying physical processes and the role of kinetic effects on the formation of excess air, we simulated the dissolution of entrapped air using both the KBD model [*Holocher et al.*, 2003] and the local equilibrium model [*Cirpka and Kitanidis*, 2001], as described in section 2.3. The parameter values used for the KBD and local equilibrium models are summarized in Table 3 ('Sand column'). The parameters r and S_g^{ini} were obtained from fitting the KBD model to the

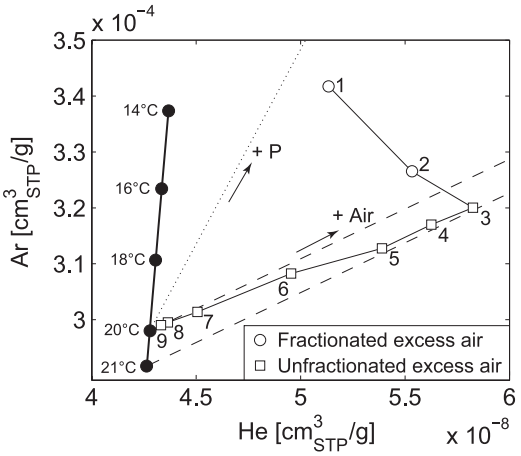

Figure 3. Measured He and Ar concentrations during the sand-column experiment. Filled circles: atmospheric solubility equilibrium at different temperatures; dashed line: addition of unfractionated air; dotted line: solubility equilibrium at increasing pressure. Samples 1 and 2 are between the lines for pure excess air and pressure enhancement, indicating fractionation with respect to the composition of atmospheric air. All other samples (3–9) contain unfractionated excess air, because their elemental composition closely follows the dashed line.

Table 3. Model Parameter Values Used in the KBD and Local Equilibrium Model Simulations[a]

Simulation			Sand Column	Unfrac. EA	Model Comparison
Model parameter			Value		Value
Flow direction			H[b]	H[b]	H, VD, VU[d]
h	Hydraulic head	[m]	1.85[e]	1[e]	1[e] (H), 0[f] (VD), 1[f] (VU)
L	Column length	[m]	1	1	1
r	Initial bubble radius	[mm]	1.5[g]	0.5	0.5
Θ	Total porosity	[−]	0.4	0.4	0.4
S_g^{ini}	Initial gas saturation	[%]	6.89[g]	4.76	4.76
T	Water temperature	[°C]	20	10	10
p_{atm}	Atmospheric pressure	[10^5 Pa]	0.969	1.013	1.013
S	Salinity	[per mille]	0	0	0
q	Darcy Velocity	[m/s]	1.18×10^{-4}	10^{-6}	10^{-4}, 10^{-5}, 10^{-6}
D	Dispersion Coefficient	[m^2/s]	2.58×10^{-6}	0	0
Inflow concentration					
	i = He	[−]	1.02	1	1
	i = Ne	[−]	1.01	1	1
	i = Ar	[−]	1.01	1	1
c_i^{in}/c_i^{eq}	i = Kr	[−]	0.99	1	1
	i = Xe	[−]	1.01	1	1
	i = N_2	[−]	1	1	1
	i = O_2	[−]	1	1	1

[a]The simulation 'Sand column' refers to the experiment conducted in this work. The simulation 'Unfrac. EA' is used to assess the formation of apparently unfractionated excess air. The parameter values used for different scenarios to compare the KBD and local equilibrium models are summarized under 'Model comparison'.
[b]H: Horizontal.
[c]VD: Vertically downward.
[d]VU: Vertically upward.
[e]Above center of column.
[f]Above top of column.
[g]Fitted parameter value.

experimental data. Figure 4 shows the simulated noble gas concentrations for the sand-column experiment using the two models.

[45] The noble gas concentrations simulated by the KBD model (Figure 4a) agree very well with those measured in the water samples from the outflow of the column. The local equilibrium model (Figure 4b), by contrast, simulated qualitatively different breakthrough curves. In particular, the local equilibrium assumption prognoses a sharp front of complete gas dissolution which was obviously not observed in the experiment. We thus conclude that kinetic effects which are included in the KBD model, but not in the local equilibrium model, were important for the gas dissolution process in the column experiment. Under the conditions of the experiment, the assumption of local equilibrium between water and entrapped air is not valid. In section 5.1, we will investigate by parameter studies under which conditions kinetic effects may be neglected.

4.2. Total Dissolved Gas Pressure

[46] Total dissolved gas pressure (TDGP) was measured during the experiment, starting at time $t = -3$ h, when the sand column was filled with air-equilibrated water (Figure 2). The increase in TDGP from $t = -3$ h to the start of the experiment at $t = 0$ h, while the water stagnated in the column and re-equilibrated with the entrapped gas phase, probably represents both the typical response time of the TDGP probes and the delay due to kinetic gas exchange between the initially air-equilibrated water and the entrapped air. Starting at time $t = 0$ h, when the water flow was initiated, the TDGP at the outflow of the column was quasi-constant, lasting until about $t = 20$ h, when the TDGP decreased. This decrease is due to the complete dissolution of the entrapped gas phase indicated by TDGP values at the outflow being identical to those at the inflow at $t > 35$ h. The time of this decrease in TDGP agrees reasonably well with the time of decrease in the noble gas supersaturations (see Figure 2). However, it occurs slightly later. The maximum TDGP relative to the atmospheric pressure of about 1.18 agrees very well with the hydraulic head of 1.85 m above the geodetic height of the sand column.

[47] We believe that the delay between the decrease in TDGP relative to the noble gas concentrations may be caused by the hydrophobicity of the silicone rubber. During gas entrapment, hydrophobic surfaces are preferential locations for the remaining gas phase which in turn leads to a longer presence of gas in contact to the TDGP probes during the experiment.

[48] Despite the mentioned delay, the results indicate that the TDGP probe is a simple, easy-to-use device to measure the total dissolved gas pressure in water samples. TDGP probes may be appropriate to estimate the amount of excess air if noble gas measurements are not available, for example in the context of the interpretation of environmental tracer data such as SF_6 as anthropogenic trace gas used for groundwater dating, which is very sensitive to the presence of excess air [*Busenberg and Plummer*, 2000]. The use of a TDGP probe to estimate excess air in the field, however, requires the consideration of the non-conservative behavior of certain gases, e.g., the consumption of oxygen [see *Manning et al.*, 2003].

5. Parameter Studies on System Behavior

5.1. Relevance of Kinetic Effects

[49] Neglecting dispersion and inter-phase mass transfer kinetics, *Cirpka and Kitanidis* [2001] analyzed the coupled

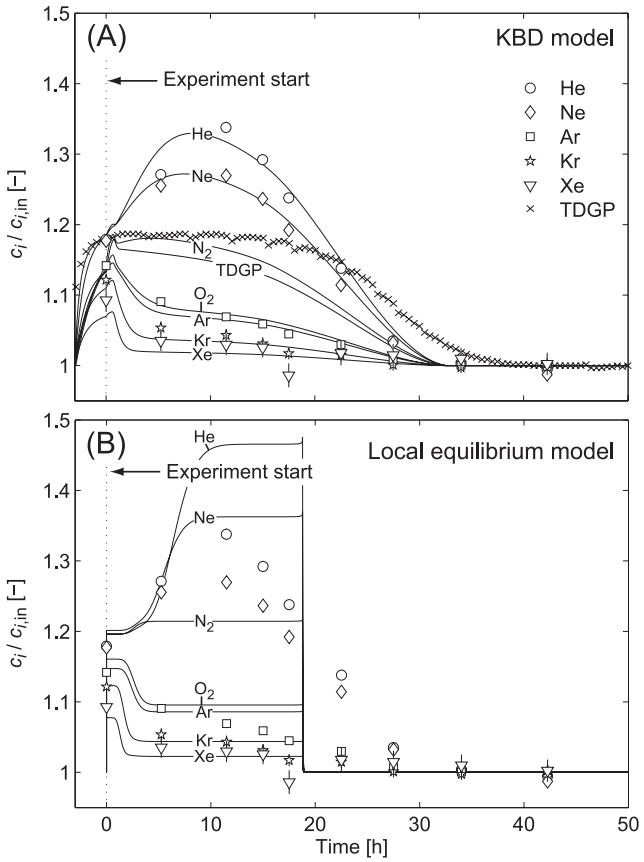

Figure 4. Measured (symbols) and modeled (solid lines) noble gas concentrations in the sand-column experiment simulated using the KBD model (a) and the local equilibrium model (b). All concentrations are normalized by the respective concentrations in the inflowing water. The dotted line denotes the start of the experiment at $t = 0$ h.

transport of the dissolved gases in the presence of an entrapped gas phase using the theory of hyperbolic systems. Each partitioning compound is characterized by its corresponding Henry's law coefficient. Transport of the various volatile compounds in the presence of an immobile gas phase is coupled via the total gas pressure, p_g, according to equation (9). Without this coupling, variations in the concentration of each dissolved gas would be propagated independently through the domain, each with its own characteristic velocity. Because of the coupling, concentration changes are split into several combinations of concentration changes traveling through the domain with a characteristic velocity. Each such traveling combination of concentration changes is denoted a concentration wave. In a system with n different gases, n waves with characteristic composition and celerity travel through the system, the last of which is associated with complete dissolution of the gas phase. Because the dissolved concentrations and partial pressures of the noble gases are very small in comparison to those of the main air constituents N_2 and O_2, variations in the noble gas concentrations have hardly any effect on the gas saturation, and therefore hardly affect the concentrations and partial pressures of the other gases. By contrast, changes in the concentrations of the main constituents N_2 and O_2 significantly affect the concentrations and partial pressures of all the other gas species.

[50] Dispersion and inter-phase mass transfer kinetics smooth the traveling waves so that distinct steps may no more be observed. This was obviously the case under the conditions of the sand-column experiment. However, if the characteristic timescale of gas transfer is small and the timescale of dispersion is large in comparison to the advective timescale, the system behavior should approach the description of advective transport coupled to instantaneous gas transfer.

[51] In the following parameter studies, we will vary the flow velocity to increase the advective timescale in order to quantify the difference in the results of the KBD and local equilibrium models. To eliminate the effect of the column length, we use the dimensionless Damköhler number Da to characterize the relative importance of kinetics in the mass transfer between water and the entrapped gas phase:

$$Da = \frac{A_b \cdot L \cdot k_i}{V_w \cdot v} \tag{21}$$

in which L is the column length, v is the seepage velocity, k_i is the mass transfer coefficient according to equation (13), and (A_b/V_w) is the specific interfacial area:

$$\frac{A_b}{V_w} = \frac{A_b}{V_b} \cdot \frac{V_b}{V_w} = \frac{3}{r} \cdot \frac{S_g}{1 - S_g} \tag{22}$$

where A_b is the surface area of the assumed gas bubble , V_b is the bubble volume, and V_w is the water volume. Substitution of equations (13) and (22) into equation (21) yields:

$$Da = \frac{3L \cdot S_g \cdot D_{w,i}}{v \cdot r \cdot (1 - S_g)} \left(\frac{1}{r} + \sqrt{\frac{v}{2\pi \cdot r \cdot D_{w,i}}} \right) \tag{23}$$

[52] Both the gas saturation S_g and bubble radius r change during the experiment. As a result, the Damköhler number also changes. For comparison purpose, all following results refer to the initial Damköhler number Da_{ini}, which is computed with the radius, gas saturation, and seepage velocity at the beginning of the experiment. Several authors report that the assumption of local equilibrium is valid for $Da > 100$ [*Brusseau*, 1992, and references therein], whereas $Da < 100$ would indicate that mass transfer is significantly controlled by kinetics.

[53] We compute the root mean square error ε to quantify the deviation of the KBD model predictions, $c_i^{KBD}(t)$, from those of the local equilibrium model, $c_i^{LE}(t)$:

$$\varepsilon = \sqrt{\frac{1}{n_i} \sum_i \frac{1}{t_{diss}^{KBD}} \int_0^{t_{diss}^{KBD}} \left(\frac{c_i^{LE}(t) - c_i^{KBD}(t)}{c_i^{LE,ini} - c_i^{eq}} \right)^2 \mathrm{d}t} \tag{24}$$

with i = He, Ne, Ar, Kr, Xe, N_2, O_2. n_i is the number of compounds i considered, $c_i^{LE,ini}$ is the concentration of compound i at $t = 0$ calculated by the local equilibrium model, and t_{diss}^{KBD} is the time at which the entire gas phase has been dissolved according to the KBD model.

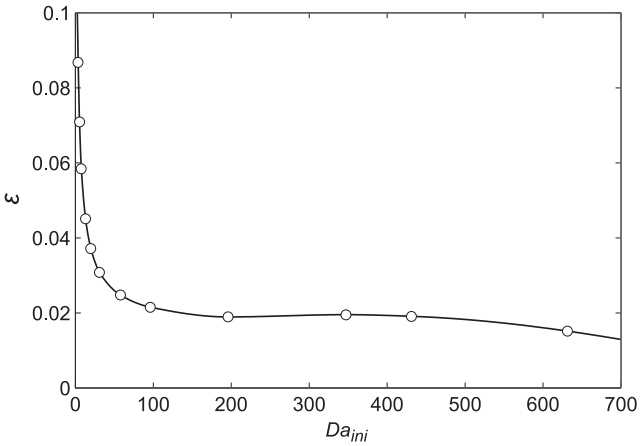

Figure 5. Comparison of the results obtained from the local equilibrium and KBD models, depicted as root mean square errors ε versus initial Damköhler numbers Da_{ini}. Significant differences between the KBD and local equilibrium model results are only obvious for $Da_{ini} < 100$.

[54] Figure 5 shows the values of ε as function of the initial Damköhler number Da_{ini}. For $Da_{ini} < 100$ the root mean square error ε is relatively large, for $Da_{ini} > 100$, the values of ε are about 0.02 and remain virtually constant for increasing values of Da_{ini}. We therefore conclude, in agreement with previous authors, that for $Da_{ini} > 100$ the KBD and local equilibrium models yield similar results, and the assumption of local equilibrium between the water and the entrapped gas phase seems to be justified.

5.2. Impact of Flow Direction

[55] Since hydrostatic pressure dominates the solubility equilibrium between water and the entrapped gas phase, the dissolution of entrapped gas depends significantly on flow direction. If the direction of flow is horizontal, the hydrostatic pressure is almost constant along a short flow distance, and hence the gas equilibrium is virtually identical along the same distance. In contrast, in the case of vertical flow, there is a hydrostatic pressure gradient either in the direction of flow (for vertically downward flow) or in the reverse direction (for vertically upward flow). As a result, the gas equilibrium also changes along the flow paths. The temporal characteristics of gas dissolution are therefore different for horizontal, downward, and upward flow directions.

[56] Figure 6 shows the results of simulations using the KBD and local equilibrium models for horizontal, vertically downward, and vertically upward flow. All other model parameter values are identical for all simulations (see Table 3, 'Model comparison'). For better comparability, time t is transformed to the nondimensional pore volume V_p:

$$V_p = \frac{q \cdot t}{\Theta \cdot L} \tag{25}$$

[57] Three main differences in the system behavior, caused by the orientation of flow, are obvious (see Figure 6):

[58] (i) In all simulations the supersaturations evolve into a quasi-constant, plateau-like phase which lasts for a long time period during dissolution of the gas phase. However, the behavior from the beginning of the simulation to that plateau phase is different for different flow directions. In the case of horizontal flow, there is a stepwise increase in the supersaturations of the lighter gases (He, Ne, N_2), and a stepwise decrease in the supersaturations of the heavier gases (Ar, Kr, Xe, O_2). In the case of vertically downward flow, by contrast, the supersaturations increase or decrease into the plateau phase, forming a ramp instead of a step. In the third case of vertically upward flow, the lighter gases first decrease and then increase to the plateau phase, and the heavier gases first increase and then decrease to the plateau phase.

[59] (ii) The timing of the complete dissolution of the entrapped air also depends strongly on flow direction. For horizontal flow direction, the relationship between complete bubble dissolution in the flow direction and the distance traveled is linear. In the case of vertically downward flow, complete bubble dissolution takes place almost simultaneously throughout the column. Only very close to the inflow does the entrapped air dissolve significantly faster than in the rest of the column. In the case of vertically upward flow, the time of complete gas dissolution increases faster than linearly with distance.

[60] (iii) The evolution of the gas saturation is also different for horizontal and vertical flow directions. In the case of horizontal flow, the gas saturation remains almost constant until abrupt, complete gas dissolution. In the case of vertically downward flow, the gas saturation decreases linearly with time, whereas vertically upward flow leads to an increase in gas saturation close to the top of the column until instantaneous dissolution of the gas phase occurs. This is so because the equilibrium concentration of the gaseous compounds decreases with travel distance. As a consequence, a water parcel picks up volatile compounds near the inlet and partially releases it again further toward the top of the column.

5.3. Apparently Unfractionated Excess Air

[61] An unexpected finding of our experiments is that all samples taken in the outflow of the column at $t \gtrapprox$ 6 h contained apparently unfractionated excess air (samples 3–9 in Figure 3, see above), although an entrapped and progressively dissolving gas phase was definitely present during that time. As already stated, unfractionated excess air is usually attributed to the complete dissolution of entrapped air [*Heaton and Vogel*, 1981]. Our observation casts doubts on the interpretation of noble gas data from typical field samples where the flow and transport system is barely known.

[62] During the experiment, an entrapped gas phase was present and this gas phase has undergone fractionation as indicated by the change of composition in the course of the experiment. Apparently, the composition of the observed gas excess, and therefore the composition of the gas flux out of the entrapped gas bubbles into the water, was very similar to the composition of free atmospheric air. After an initial phase, the poorly soluble noble gases He and Ne had accumulated in the remaining gas phase, while the concentrations of the more soluble compounds Ar, Kr, and Xe had decreased. In the remaining time of gas dissolution, the change in partial pressure in turn partially compensated the differences in gas solubilities, leading to the generation of apparently unfractionated excess air.

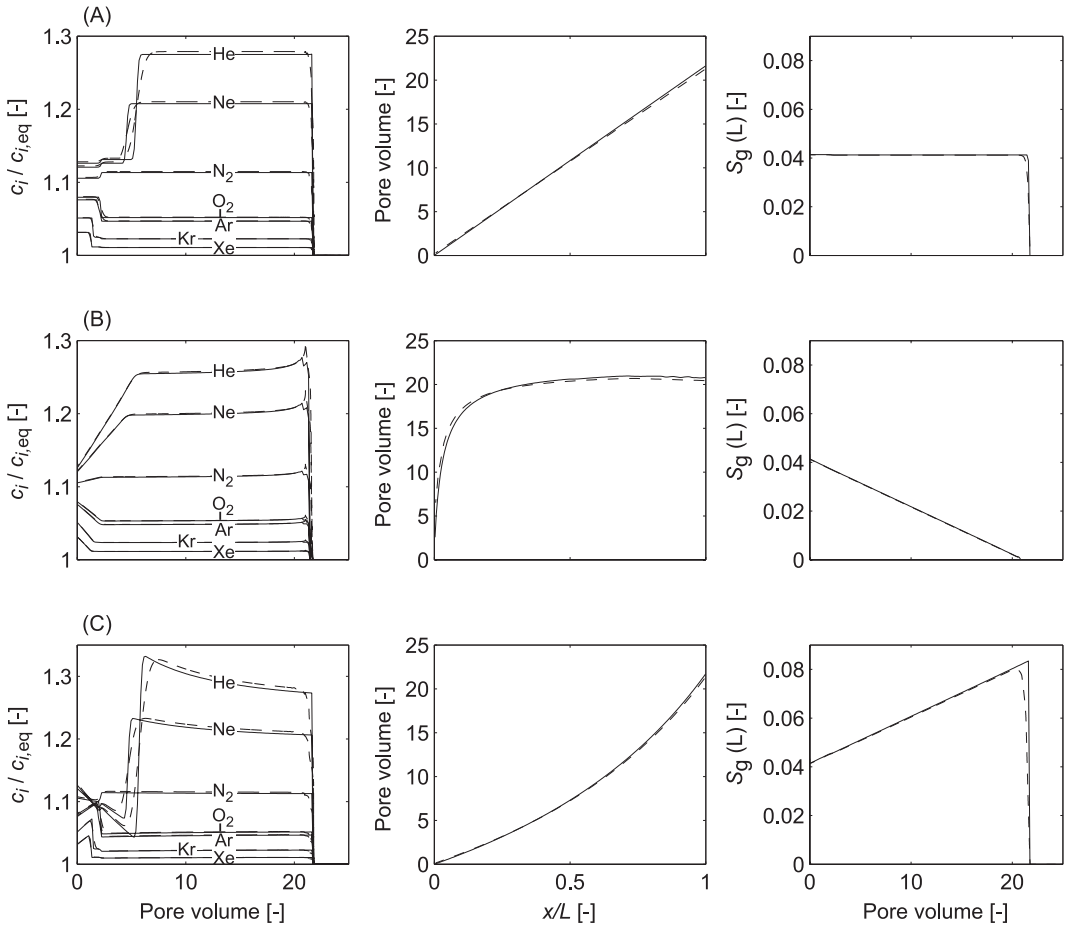

Figure 6. Effects of horizontal and vertical flow directions, simulated using the local equilibrium model (solid lines) and the KBD model (dashed lines): (a) horizontal flow, (b) vertically downward flow, and (c) vertically upward flow, for Da_{ini} = 365 ($q = 10^{-6}$ m/s, $\tau \approx 100$ h). The graphs in the middle panel show the number of pore volumes that are required until complete gas-phase dissolution is achieved as a function of the relative flow distance *x/L*. The graphs in the right-hand panel show the gas saturation at the end of the column.

[63] To verify this hypothesis, we calculated the elemental ratios of the gas excess component, defined as the difference between the measured concentration and the atmospheric equilibrium concentration of the gas considered, and compared them with the partial pressure ratios in atmospheric air (Figures 7a and 7b). Because the local equilibrium model exhibits clear fronts, we performed the simulations with the latter model using the parameter values given in Table 3 (column 'Unfrac. EA'). Note that this simulation and the results discussed below do not refer to the experiment described in section 4 but represent generic simulations performed to illustrate the formation of apparently unfractionated excess air in the presence of a continuously dissolving gas phase.

[64] For less than about 6 pore volumes, phase 1 of the simulation (see Figure 7), the elemental ratios of the gas excess vary strongly and are significantly different from the atmospheric ratios, forcing the formation of fractionated excess air. After about 6 pore volumes, in phase 2 of the simulation, the elemental ratios in the gas excess are almost constant and in parts very similar to the partial pressure ratios in the atmosphere. The more similar the gases are in terms of solubility, the more the elemental ratios of the gas excess agree with the atmospheric ratios (e.g., He/Ne, Kr/Xe, Ar/O_2). The ratios of gases with more different solubilities differ considerably more from the atmospheric ratios (e.g., He/Xe). Figures 7c, 7d, and 7e show the fitted parameters T_{ng} (noble gas temperature), A (amount of entrapped air), F (fractionation factor), q_{CE} (pressure factor) obtained from the simulated noble gas concentrations, using the CE model. In phase 1, the CE model proposes the formation of fractionated excess air, indicated by $F > 0$. The fractionation then decreases until unfractionated excess air is formed in phase 2; i.e., the value of F decreases to 0 at the end of phase 1. The noble gas temperature T_{ng} (Figure 7c) also varies considerably during phase 1 in response to the variations in the elemental ratios of the gas excess. That is, a relative surplus of the more soluble and more temperature-dependent noble gases, e.g., a low ratio of He/Xe, is compensated for by a low noble gas temperature, and vice versa. In phase 2, the noble gas temperature varies only slightly and remains almost constant with time. The relative surplus of the least soluble noble gases He and Ne (see Figure 7b) is compensated for by a noble gas temperature that is slightly above the 'real' water temperature of 10°C set for the simulation.

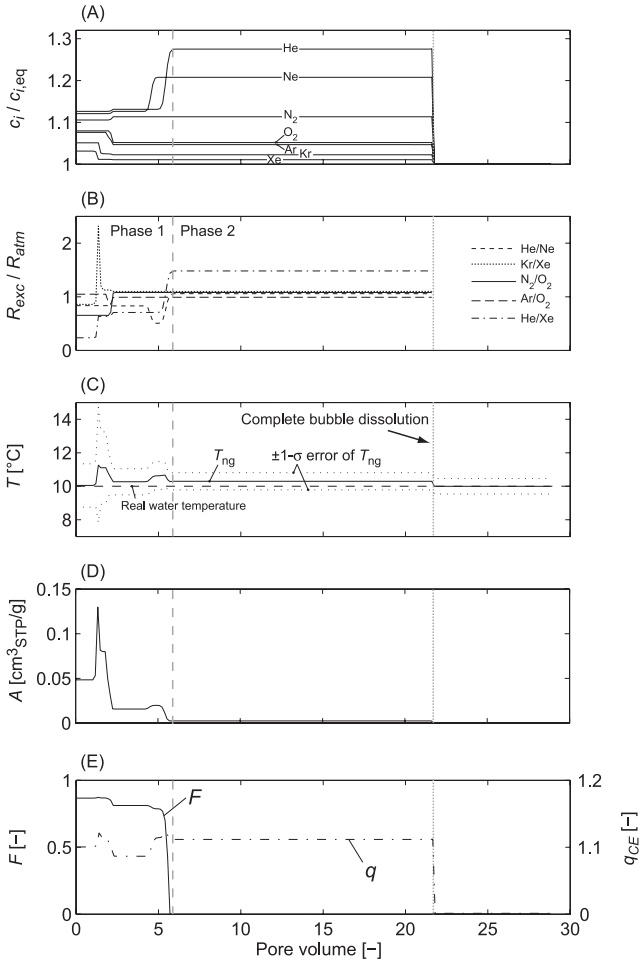

Figure 7. (a) Relative concentration during the dissolution of entrapped air as calculated by the local equilibrium model. (b) Elemental ratios of the gas excess relative to the partial pressure ratios of atmospheric air. (c) Noble gas temperature T_{ng}, (d) excess air A, and (e) fractionation factor F and pressure factor q_{CE} determined by the CE model [*Aeschbach-Hertig et al.*, 2000].

[65] The fitted parameter A reflects the correct gas saturation of 5% only at the very beginning of the dissolution process. Especially during phase 2, when the excess air component seems to be unfractionated, the CE model (or the special UA-case of the CE model for $F = 0$) proposes values of A, which are much smaller than the real entrapped gas volume. As shown in section 5.2, the real gas saturation at the outflow of the column remains at about 5% until complete dissolution of the gas phase occurs. We conclude therefore that the CE model underestimates the entrapped air volume significantly during the long lasting phase 2 with almost constant noble gas concentrations. It is important to note that the misleading gas saturation determined by the CE model is based on the incorrect assumption that the entrapped gas phase has the same composition as atmospheric air, which is only true at the beginning of the dissolution process when the model yield the correct value for A. Nevertheless, since the CE model is routinely applied to interpret noble gas concentrations in groundwater, it is very important to note that, in the case of apparently unfractionated excess air, the fitted value for the entrapped air volume A is not at all identical to the real entrapped air volume, and caution has to exercised when interpreting the CE model parameter A.

[66] A pressure factor q_{CE} of 1.1 is expected corresponding to the hydraulic head of 1 m. The pressure factor q_{CE} closely reflects the correct hydrostatic pressure during the entire process of gas dissolution (see Figure 7e). Therefore the pressure factor q_{CE} seems to be suitable to estimate the hydrostatic pressure exerted on the system during the formation of excess air. Several authors proposed the use of excess air as a proxy for pressure conditions during groundwater recharge, which are mainly controlled by groundwater table fluctuations [e.g., *Stute and Talma*, 1998; *Kulongoski et al.*, 2004; *Ingram et al.*, 2007; *Manning and Caine*, 2007]. Excess Ne (ΔNe), which is often used to express the amount of excess air and as a proxy for hydrostatic pressure, only reflects the correct pressure during phase 1 of the gas dissolution process (see Figure 7a) but ΔNe overestimates the pressure by a factor of $\sim$2 during phase 2. The pressure factor q_{CE} therefore seems to provide the more reliable estimate of the hydrostatic pressure, particularly during phase 2 of the process of gas dissolution. It should be noted that the pressure factor q_{CE} only yields a correct estimate of the pressure in the case of local solubility equilibrium. If local equilibrium is not achieved, q_{CE} underestimates the pressure. However, because the local equilibrium assumption seems to be valid under most natural conditions (see below), q_{CE} can be used to infer the hydrostatic pressure exerted on the system, i.e., q_{CE} may be used as a proxy for groundwater table fluctuations.

[67] Importantly, during phase 2, the excess air component seems to be unfractionated according to the parameter fit using the CE model ($F = 0$), adjusting the noble gas temperature to a value which is slightly above the assumed water temperature of the numerical simulation (10°C). Such a slight increase in the noble gas temperature was also observed in the water samples from the sand-column experiment (see section 4.1). The difference between noble gas and real water temperature, however, is smaller than the error of the noble gas temperature calculation using the CE model. However, if the hydrostatic pressure exceeds about 0.2–0.3 bar (corresponding to a rise of the groundwater table of about 2–3 m), the relative surplus of the least soluble, light noble gases becomes too large to be compensated for by the CE model, adjusting the determined noble gas temperature to higher values; i.e., no statistically acceptable fit for T_{ng}, A, and F can be achieved. The fact that most groundwater samples from field studies yield acceptable fits using the CE model may indicate that such pressure conditions (i.e., large groundwater table fluctuations) are rare or that phase 2 is seldom reached in natural systems.

6. Discussion and Conclusions

[68] The sand-column experiments conducted in combination with simulations using the KBD and local equilibrium models show that inter-phase mass transfer kinetics play an important role in the dissolution of entrapped air for small values of the initial Damköhler number $Da_{ini} < 100$; i.e., in the case of large flow velocities or small travel distances through the quasi-saturated zone. For large values

of $Da_{ini} > 100$, both models yield similar results; i.e., the assumption of local equilibrium between the water and gas phases is appropriate for low flow velocities and large distances.

[69] Groundwater table fluctuations in temperate climate zones are usually within the range of a few meters at most, and the thickness of the quasi-saturated zone is therefore limited. Thus for vertical flow, the characteristic length scale used in the calculation of the Damköhler number is limited. Under these conditions, flow velocities of 10^{-4} m/s or larger require that the kinetics of gas dissolution are accounted for, whereas they may be neglected for velocities smaller than 10^{-5} m/s. For horizontal flow, the travel distance in the quasi-saturated zone can be considerably larger, thus extending the range in which the local equilibrium model is a reasonable assumption for the dissolution of entrapped gas in natural porous media.

[70] For excess-air formation by regional groundwater recharge, where horizontal velocities are in the order of 1 m/d and horizontal distances are in the order of hundreds of meters, Damköhler numbers of $Da > 100$ are most likely to be reached. The related vertical velocities are in the order of $\sim$1 m per year with vertical distances of a few meters the most. Again, this points to Damköhler numbers of $Da > 100$. That is, we assume that the local equilibrium assumption is valid for typical situations of regional groundwater recharge. This is different for gas exchange between river infiltrate and entrapped gas in the hyporheic zone of a river with a natural river bed. Residence times in the hyporheic zone are typically in the order of a few hours, leading to values of Da considerably smaller than 100. This implies that for typical situations of hyporheic exchange clear non-equilibrium partitioning conditions prevail.

[71] If the flow direction is predominantly horizontal, the combination of advection-dominated transport and local gas-water partitioning in equilibrium leads to sharp fronts traveling through the quasi-saturated domain. Continuous concentration changes may be caused by inter-phase mass transfer kinetics. However, they can also be caused by transport coupled to equilibrium partitioning if the flow direction is downward. In case of upward flow, the dissolution of entrapped gas at depth may be combined with intermediate increase of gas saturation at low depth. The dependence of partitioning equilibrium on hydrostatic pressure should be accounted for in the design of experiments. *Holocher et al.* [2002] performed laboratory experiments with downward flow and compared the results to large-scale experiments in a sand filter where the flow direction was also downward. *Geistlinger et al.* [2005], by contrast, performed experiments in vertical columns with upward flow in order to mimic conditions during air-sparging, where flow typically is horizontal. The different flow direction may complicate the transfer of laboratory experiments to field conditions.

[72] Although a majority of groundwater samples contain excess air which is fractionated with respect to the composition of free atmospheric air, unfractionated excess air is also frequently found in groundwater samples and is usually attributed to the complete dissolution of entrapped air. For example, *Ingram et al.* [2007] report unfractionated excess air from a sandstone aquifer system in the East of England. The CE model was used to interpret the measured noble gas concentrations and the fractionation factor F was found to be 0 for most samples, i.e., the excess air component is (apparently) unfractionated. In most of the samples, the fit of the CE model lead to small values of A, expressing the amount of entrapped, and completely dissolved air ($2\ \mathrm{cm^3_{STP}/kg} \lessapprox A \lessapprox 5\ \mathrm{cm^3_{STP}/kg}$). The CE model interpretation, i.e., the special UA-case of the CE model for $F = 0$, therefore suggests a residual gas saturation of only 0.2–0.5%, which conflicts with observations of typical entrapped air volume ratios ranging from a few per cent up to several tens of per cent [*Christiansen*, 1944; *Fayer and Hillel*, 1986; *Stonestrom and Rubin*, 1989; *Faybishenko*, 1995; *Wang et al.*, 1998].

[73] The results of our study give a new interpretation of apparently unfractionated excess air in conjunction with small fitted values of A. In our experiment and in our model simulations, such a combination occurred without complete dissolution of entrapped air. During the progressive dissolution of the entrapped gas phase, fractionated excess air was only produced during the beginning of the dissolution process. Apparently unfractionated excess air was generated during a predominant period of time during which the gas phase evolved in such a manner that the inter-phase mass fluxes of volatile compounds between the aqueous and gaseous phases showed elemental ratios that are very similar to the partial pressure ratios in atmospheric air. We conjecture that a CE-model fit with $F = 0$ and $A < 10\ \mathrm{cm^3_{STP}/kg}$ points to conditions similar to phase 2 of our study, characterized by incomplete dissolution of entrapped air in a transient state.

[74] We believe that apparently unfractionated excess air is an indicator of complete dissolution of entrapped gas only when the fitted amount of dissolved gas is in the range of reported values for residual gas saturation (i.e., $A \gg 10\ \mathrm{cm^3_{STP}/kg}$). Dissolving such amounts of entrapped gas in a closed system, as postulated by the CE model, requires a substantial increase of hydrostatic pressure. Reported fluctuations of the groundwater table, however, typically are in the range of a few meters at the most, which is confirmed by limited values of excess air ($10\% \lessapprox \Delta Ne \lessapprox 120\%$) [*Kipfer et al.*, 2002, and references therein]. With limited increase in hydrostatic pressure, it is not possible to completely dissolve several per cent of entrapped gas without continuous flushing of the porous medium by groundwater with atmospheric composition of volatile compounds. However, the ubiquitous presence of excess air in most aquifers suggests that complete dissolution of entrapped air bubbles by flushing rarely occurs under natural conditions.

[75] In natural aquifers, the ratio of flow velocity (and hence the residence time within the quasi-saturated zone) to the frequency of water table fluctuations most likely determines whether fractionated or apparently unfractionated excess air is produced. That is, if the flow velocity is high, the time of phase 1 (cf. Figure 7), during which fractionated excess air is produced, is relatively short. In this case, the probability of observing fractionated excess air is high only if the groundwater table fluctuates frequently. By contrast, if the flow velocity is very low, phase 1 lasts longer, so that fractionated excess air is more likely to be observed also in systems with slowly fluctuating groundwater table.

[76] The mechanism proposed here to interpret the apparent fractionation F and associated amount A of entrapped gas

needs further confirmation from field measurement under natural conditions. In the standard case of environmental-tracer studies, only a few samples are taken and analyzed for noble-gas concentrations. As we have shown, the parameters determined by fitting the CE model to such data change with time when the noble gas compounds undergo gas transfer coupled to advective-dispersive transport. In typical field situations, it is not known to which time phase of the gas dissolution process a particular sample is related to. Samples of larger groundwater age most likely reflect mixtures of water samples related to particular time phases. Under these conditions, we see difficulties in interpreting the apparent values of F and A. The pressure factor q_{CE}, by contrast, seems to provide a reasonable estimate of the hydrostatic pressure acting on the system during the formation of excess air. The noble gas temperature T_{ng} also appears to be close to the real temperature at the time of gas dissolution, even though its derivation is based on the conceptually incorrect assumption of stagnant water. That is, T_{ng} determined by the CE model may be used for paleo-climate reconstruction without introducing systematic bias [e.g., *Aeschbach-Hertig et al.*, 2000], provided that the composition of the dissolving gas phase is similar to that of the atmosphere.

[77] **Acknowledgments.** This work was supported by the Swiss National Science Foundation (grant 200020-107489/1). We thank Werner Aeschbach-Hertig and two anonymous reviewers for their constructive remarks helping to improve the paper.

References

Aeschbach-Hertig, W., F. Peeters, U. Beyerle, and R. Kipfer (1999), Interpretation of dissolved atmospheric noble gases in natural waters, *Water Resour. Res.*, *35*(9), 2779–2792.

Aeschbach-Hertig, W., F. Peeters, U. Beyerle, and R. Kipfer (2000), Palaeotemperature reconstruction from noble gases in ground water taking into account equilibration with entrapped air, *Nature*, *405*, 1040–1044.

Aeschbach-Hertig, W., U. Beyerle, J. Holocher, F. Peeters, and R. Kipfer (2002), Excess air in groundwater as a potential indicator of past environmental changes, in *Study of Environmental Change Using Isotope Techniques*, *C&S Papers Series*, vol. 13/P, edited by IAEA, pp. 174–183, IAEA, Vienna.

Amos, R. T., and K. U. Mayer (2006), Investigating the role of gas bubble formation and entrapment in contaminated aquifers: Reactive transport modelling, *J. Contam. Hydrol.*, *87*(1–2), 123–154.

Balcke, G. U., S. Meenken, C. Hoefer, and S. E. Oswald (2007), Kinetic gas-water transfer and gas accumulation in porous media during pulsed oxygen sparging, *Environ. Sci. Technol.*, *41*(12), 4428–4434.

Ballentine, C. J., and C. M. Hall (1999), Determining paleotemperature and other variables by using an error-weighted, nonlinear inversion of noble gas concentrations in water, *Geochim. Cosmochim. Acta*, *63*(16), 2315–2336.

Beyerle, U., W. Aeschbach-Hertig, D. M. Imboden, H. Baur, T. Graf, and R. Kipfer (2000), A mass spectrometric system for the analysis of noble gases and tritium from water samples, *Environ. Sci. Technol.*, *34*(10), 2042–2050.

Beyerle, U., J. Rüedi, M. Leuenberger, W. Aeschbach-Hertig, F. Peeters, R. Kipfer, and A. Dodo (2003), Evidence for periods of wetter and cooler climate in the Sahel between 6 and 40 kyr BP derived from groundwater, *Geophys. Res. Lett.*, *30*(4), 1173, doi:10.1029/2002GL016310.

Brusseau, M. L. (1992), Rate-limited mass transfer and transport of organic solutes in porous media that contain immobile immiscible organic liquid, *Water. Resour. Res.*, *28*(1), 33–45.

Busenberg, E., and N. L. Plummer (2000), Dating young groundwater with sulfur hexafluoride: Natural and anthropogenic sources of sulfur hexafluoride, *Water Resour. Res.*, *36*(10), 3011–3030.

Christiansen, J. E. (1944), Effect of entrapped air upon the permeability of soils, *Soil Sci.*, *58*(5), 355–365.

Cirpka, O. A., and P. K. Kitanidis (2001), Transport of volatile compounds in porous media in the presence of a trapped gas phase, *J. Contam. Hydrol.*, *49*, 263–285.

Clever, H. L. (1979), *Krypton, Xenon and Radon-Gas Solubilities*, *Solubility Data Series*, vol. 2, Pergamon Press, Oxford.

Epstein, P. S., and M. S. Plesset (1950), On the stability of gas bubbles in liquid-gas solutions, *J. Chem. Phys.*, *18*(11), 1505–1509.

Faybishenko, B. A. (1995), Hydraulic behavior of quasi-saturated soils in the presence of entrapped air: Laboratory experiments, *Water Resour. Res.*, *31*(10), 2421–2435.

Fayer, M. J., and D. Hillel (1986), Air encapsulation: 1. Measurement in a field soil, *Soil Sci. Soc. Am. J.*, *50*, 568–572.

Geistlinger, H., A. Beckmann, and D. Lazik (2005), Mass transfer between a multicomponent trapped gas phase and a mobile water phase: Experiment and theory, *Water Resour. Res.*, *41*, W11408, doi:10.1029/2004WR003885.

Heaton, T. H. E., and J. C. Vogel (1981), "Excess air" in groundwater, *J. Hydrol.*, *50*, 201–216.

Holocher, J. (2002). Investigations of gas exchange in quasi-saturated porous media using noble gases as conservative tracers. Diss. ETH No. 14588, ETH Zürich.

Holocher, J., F. Peeters, W. Aeschbach-Hertig, M. Hofer, M. Brennwald, W. Kinzelbach, and R. Kipfer (2002), Experimental investigations on the formation of excess air in quasisaturated porous media, *Geochim. Cosmochim. Acta*, *66*(23), 4103–4117.

Holocher, J., F. Peeters, W. Aeschbach-Hertig, W. Kinzelbach, and R. Kipfer (2003), Kinetic model of gas bubble dissolution in groundwater and its implications for the dissolved gas composition, *Environ. Sci. Technol.*, *37*(7), 1337–1343.

Ingram, R. G. S., K. M. Hiscock, and P. F. Dennis (2007), Noble gas excess air applied to distinguish groundwater recharge conditions, *Environ. Sci. Technol.*, *41*, 1949–1955.

Johnson, P. C. (1998), Assessment of the contributions of volatilization and biodegradation to in situ air sparging performance, *Environ. Sci. Technol.*, *32*(2), 276–281.

Kipfer, R., W. Aeschbach-Hertig, F. Peeters, and M. Stute (2002), Noble gases in lakes and ground waters, in Noble gases in geochemistry and cosmochemistry, *Rev. Mineral. Geochem.*, vol. 47, edited by D. Porcelli, C. Ballentine, and R. Wieler, pp. 615–700. Mineralogical Society of America, Geochemical Society, Washington, DC.

Klump, S., Y. Tomonaga, P. Kienzler, T. Kinzelbach, W. Baumann, D. M. Imboden, and R. Kipfer (2007), Field experiments yield new insights into gas exchange and excess air formation in natural porous media, *Geochim. Cosmochim. Acta*, *71*(6), 1385–1397.

Kreft, A., and A. Zuber (1978), On the physical meaning of the dispersion equation and its solutions for different initial and boundary conditions, *Chem. Eng. Sci.*, *33*, 1471–1480.

Kulongoski, J. T., D. R. Hilton, and E. T. Selaolo (2004), Climate variability in the Botswana Kalahari from late Pleistocene to the present day, *Geophys. Res. Lett.*, *31*, L10204, doi:10.1029/2003GL019238.

Lagarias, J. C., J. A. Reeds, M. H. Wright, and P. Wright (1998), Convergence properties of the Nelder-Mead Simplex Method in low dimensions, *SIAM J. Control Optim.*, *9*(1), 112–147.

Manning, A. H., and J. S. Caine (2007), Groundwater noble gas, age, and temperature signatures in an Alpine watershed: Valuable tools in conceptual model development, *Water Resour. Res.*, *43*, W04404, doi:10.1029/2006WR005349.

Manning, A. H., D. K. Solomon, and A. L. Sheldon (2003), Applications of a total dissolved gas pressure probe in ground water studies, *Ground Water*, *41*(4), 440–448.

Mazor, E. (1972), Paleotemperatures and other hydrological parameters deduced from gases dissolved in groundwaters, Jordan Rift Valley, Israel, *Geochim. Cosmochim. Acta*, *36*(12), 1321–1336.

Mercury, L., D. L. Pinti, and H. Zeyen (2004), The effect of the negative pressure of capillary water on atmospheric noble gas solubility in ground water and palaeotemperature reconstruction, *Earth Planet. Sci. Lett.*, *223*, 147–161.

Oster, H., C. Sonntag, and K. O. Münnich (1996), Groundwater age dating with chlorofluorocarbons, *Water Resour. Res.*, *32*(10), 2989–3001.

Schlosser, P., M. Stute, C. Dörr, C. Sonntag, and K. O. Münnich (1988), Tritium/3He-dating of shallow groundwater, *Earth Planet. Sci. Lett.*, *89*(3–4), 353–362.

Stonestrom, D. A., and J. Rubin (1989), Water content dependence of trapped air in two soils, *Water Resour. Res.*, *25*(9), 1947–1958.

Stute, M., and A. S. Talma (1998). Glacial temperatures and moisture transport regimes reconstructed from noble gases and $\delta^{18}O$, Stampriet

Aquifer, Namibia, in *Isotope Techniques in the Study of Environmental Change*, pp. 307–318, IAEA, Vienna.

Stute, M., M. Forster, H. Frischkorn, A. Serejo, J. F. Clark, P. Schlosser, W. S. Broecker, and G. Bonani (1995), Cooling of tropical Brazil (5°C) during the Last Glacial Maximum, *Science*, *269*, 379–383.

Wang, Z., J. Feyen, M. T. van Genuchten, and D. R. Nielsen (1998), Air entrapment effects on infiltration rate and flow instability, *Water Resour. Res.*, *34*(2), 213–222.

Weiss, R. F. (1970), The solubility of nitrogen, oxygen and argon in water and seawater, *Deep Sea Res.*, *17*(4), 721–735.

Weiss, R. F. (1971), Solubility of helium and neon in water and seawater, *J. Chem. Eng. Data*, *16*(2), 235–241.

Weiss, R. F., and T. K. Kyser (1978), Solubility of krypton in water and seawater, *J. Chem. Eng. Data*, *23*(1), 69–72.

Williams, M. D., and M. Oostrom (2000), Oxygenation of anoxic water in a fluctuating water table system: An experimental and numerical study, *J. Hydrol.*, *230*(1–2), 70–85.

O. A. Cirpka and R. Kipfer, Swiss Federal Institute of Aquatic Science and Technology (Eawag), Water Resources and Drinking Water, Überlandstrasse 133, 8600 Dübendorf, Switzerland. (olaf.cirpka@eawag.ch; rolf.kipfer@eawag.ch)

S. Klump, EBA Engineering Consultants Ltd., Calcite Business Centre, Unit 6, 151 Industrial Road, Whitehorse, Yukon Y1A 2V3, Canada. (sklump@eba.ca)

H. Surbeck, Centre of Hydrogeology, University of Neuchâtel, Rue Emile-Argand 11, 2009 Neuchâtel, Switzerland. (heinz.surbeck@unine.ch)